Electr Eng (2007) 89: 353–361
DOI 10.1007/s00202-006-0019-1

ORIGINAL PAPER

N.L. Tsitsas · E.G. Alivizatos · H.T. Anastassiu
D.I. Kaklamani

Optimization of the method of auxiliary sources (MAS) for oblique incidence scattering by an infinite dielectric cylinder

Received: 4 October 2005 / Accepted: 9 February 2006 / Published online: 11 April 2006

Abstract The analytic inversion of the Method of Auxiliary Sources (MAS) matrix plays an important role in the rigorous investigation of the accuracy of the method. In this paper we investigate the accuracy of MAS when the method is applied to plane wave scattering under oblique incidence by an infinite, dielectric circular cylinder. For this scattering configuration, we prove that the MAS matrix is analytically invertible and hence obtain a concrete expression for the discretization error. A basic contribution of this paper lies in the analytic determination of the auxiliary sources' locations, for which the corresponding system's matrix becomes singular. Furthermore, we calculate the computational error resulting from numerical matrix inversion, and compare it to the analytical error. The dependence of both types of errors on the angle of incidence and on the dielectric permittivity is investigated. Finally, error minimization indicates the auxiliary sources' optimal location.

Keywords Electromagnetic scattering · Oblique incidence · MAS · Dielectric cylinder · Error estimation

1 Introduction

The relative advantages and disadvantages of the Method of Auxiliary Sources (MAS), when compared to standard integral equation techniques in computational Electromagnetics, have been meticulously documented in the bibliography [1–8]. In particular, in [8] it was explicitly demonstrated that MAS offers significant computational cost reduction with respect to the Moment Method. Although MAS offers algorithmic simplicity and low computational cost, its applicability to specific scattering and radiation problems may become cumbersome, due to poor robustness. No generally reliable procedure is known for the successful location of the auxiliary sources (ASs) inside the problem domain, and the immediate consequence of this fact is a potential MAS inadequacy to efficiently satisfy the appropriate boundary conditions. The only general requirement is that the ASs should enclose all singularities of the scattered field's analytical continuation in the scatterer's interior [3–5]. However, since in a generic scattering geometry the singularities of the scattered field are not known, the above requirement provides limited information for practical purposes.

The optimal location of the ASs with respect to the minimization of the boundary condition error involved in the MAS solution for particular scattering geometries is investigated in [9–16]. More precisely, plane wave scattering from a perfectly conducting (PEC) infinite circular cylinder was carried out in [9] and [10] for normal incidence, while in [11] the conclusions derived were extended to oblique incidence. In [12] and [13] the MAS accuracy and optimization for normally incident plane wave scattering from an impedance and a dielectric circular cylinder were fully investigated, whereas different approaches were utilized in [14–16] for conducting, impedance and dielectric cylinders. In [9–13] it was observed that, irrespective of the cylinder's material, the circular cross section of the structure leads to a circulant (or composed of circulant blocks) MAS matrix, which is analytically invertible via eigenvalue analysis. Exact expressions for the expected discretization error were derived and compared to the actual numerical error associated with a LU matrix decomposition and inversion. The condition number was compactly expressed as well, whereas resonance effects were also pinpointed.

The above considerations motivate an extension of MAS optimization to more generic configurations. If MAS is finally optimized for a generic scatterer, the number of

N.L. Tsitsas (✉) · E.G. Alivizatos · D.I. Kaklamani
School of Electrical and Computer Engineering,
National Technical University of Athens,
Heroon Polytechniou 9, 15773 Zografou,
Athens, Greece
E-mail: ntsitsas@esd.ntua.gr
Tel.: +30-2107722467
Fax: +30-2107721092

H.T. Anastassiu
Electronics Engineering Department,
Hellenic Aerospace Industry,
PO Box 23, 32009, Schimatari-Tanagra,
Viotia, Greece

unknowns it requires may be orders of magnitude less than the moment method, and this feature will facilitate the analysis of extremely large scatterers. To achieve this goal, a complete investigation of some canonical configurations is essential before generalizing the procedure to arbitrary geometries. The purpose of this article is the completion of the work performed in [9–13], describing MAS error estimation for the most general case of plane wave illumination (oblique incidence) on an infinite, dielectric circular cylinder. The method invoked requires a set of ASs dissimilar to the one in the normal incidence case [13], and full vector wave analysis must be implemented for the calculation of the radiated fields. Furthermore, the resulting MAS matrix is composed of 4×4 circulant blocks and a novel technique is proposed towards its analytical inversion.

The paper is organized as follows: Sect. 2 presents the formulation of the problem and the analytical inversion of the MAS linear system, while Sect. 3 presents the derivation of the analytical error expressions. Section 4 presents numerical results while optimization issues are thoroughly discussed. Section 5 summarizes and concludes the article.

An $e^{j\omega t}$ time convention is assumed and suppressed throughout the paper.

2 Analytical considerations

Assume an infinite, circular dielectric cylinder of radius b and relative dielectric permittivity ε_r, located in free space with wavenumber k_0 and intrinsic impedance Z_0. The structure is illuminated by a transverse magnetic (TM^z) plane wave (with respect to the z-axis) impinging from an elevation angle θ_i (see Fig. 1). The incident wavevector is assumed to lie on the xOz plane, without loss of generality. Under these assumptions, the incident electromagnetic field at an arbitrary point (ρ, φ, z) is fully determined by the z-component of its electric field [17]

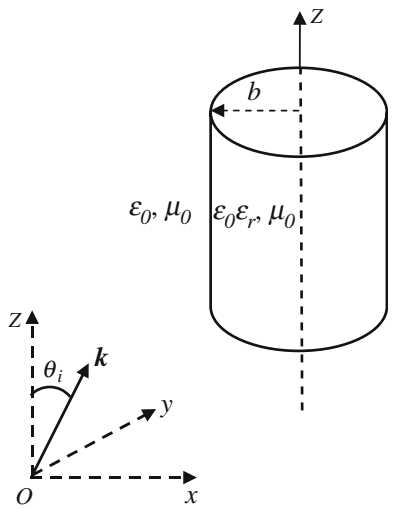

Fig. 1 Geometry of the scattering problem

$$E_z^{\text{inc}}(\mathbf{r}) = E_0 \exp\{-j\mathbf{k}\cdot\mathbf{r}\} \tag{1}$$

where

$$\mathbf{r} = \rho\,\cos\varphi\,\hat{\mathbf{x}} + \rho\,\sin\varphi\,\hat{\mathbf{y}} + z\,\hat{\mathbf{z}} \tag{2}$$

$$\mathbf{k} = k_x\hat{\mathbf{x}} + k_z\hat{\mathbf{z}} = k_0\sin\theta_i\hat{\mathbf{x}} + k_0\cos\theta_i\hat{\mathbf{z}} \tag{3}$$

are the observation vector and the incident wavevector respectively and E_0 is the amplitude of the z component of the incident electric field.

The MAS solution is constructed, by considering two fictitious auxiliary surfaces S^1 and S^0, both conformal to the actual boundary S [6]. Surface S^1 is located in the scatterer's interior, and has a circular cross section of radius $a_1 < b$, while surface S^0 is located in the scatterer's exterior and has a circular cross section of radius $a_0 > b$. Thus, the auxiliary surfaces are assumed to be cylinders of radii a_1 and a_0 respectively, each hosting a number of N ASs (see Fig. 2).

According to the MAS fundamental concept, the first set of ASs located on S^1 radiates in free space in the absence of the dielectric scatterer, while the second set of ASs located on S^0 radiates inside an infinite space filled by the material of the dielectric scatterer. The scattered field is described as a weighted superposition of the fields radiated by the first set of ASs, whereas the field inside the scatterer is described as a weighted superposition of the fields radiated by the second set of ASs.

The n-th AS ($1 \le n \le N$) on the surfaces S^1 and S^0 is assumed to model the current distribution:

$$\mathbf{I}_n^1(\rho', \phi', z') = \left(A_n\hat{\boldsymbol{\varphi}} + B_n\hat{\mathbf{z}}\right)\frac{\delta(\phi'-\phi_n)\delta(\rho'-a_1)}{\rho'}\mathrm{e}^{-jk_z z'} \tag{4}$$

$$\mathbf{I}_n^0(\rho', \phi', z') = \left(C_n\hat{\boldsymbol{\varphi}} + D_n\hat{\mathbf{z}}\right)\frac{\delta(\phi'-\phi_n)\delta(\rho'-a_0)}{\rho'}\mathrm{e}^{-jk_z z'} \tag{5}$$

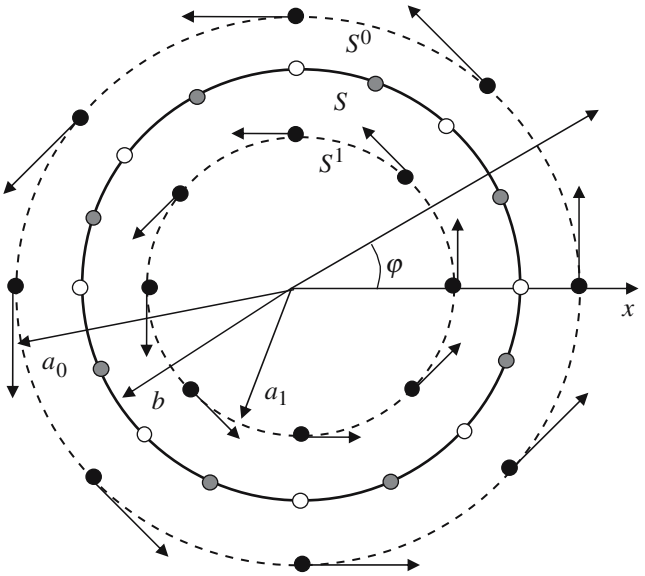

Fig. 2 Location of the sources. *Black bullets and arrows* represent Auxiliary Sources (*ASs*), while *white and gray bullets* represent Collocation Points (*CPs*) and Midpoints (*MPs*), respectively

where A_n, B_n, C_n, D_n are unknown current coefficients, which will be determined by the solution of the MAS linear system, and $\phi_n = n(2\pi/N)$ is the azimuth angle of the n-th AS.

The electric and magnetic fields $\mathbf{E}_n^0$ and $\mathbf{H}_n^0$ radiated by the interior sources are computed by using the integral operator

$$\begin{bmatrix} \mathbf{E}_n^0(\mathbf{r}) \\ \mathbf{H}_n^0(\mathbf{r}) \end{bmatrix} = \begin{bmatrix} \iiint_{\mathbb{R}^3} \bar{\bar{\mathbf{G}}}_{e\,0}(\mathbf{r},\mathbf{r}') \cdot \mathbf{I}_n^1(\mathbf{r}')\mathrm{d}\mathbf{r}' \\ \iiint_{\mathbb{R}^3} \bar{\bar{\mathbf{G}}}_{m\,0}(\mathbf{r},\mathbf{r}') \cdot \mathbf{I}_n^1(\mathbf{r}')\mathrm{d}\mathbf{r}' \end{bmatrix} \tag{6}$$

with kernel the free space dyadic electric and magnetic Green's function $\bar{\bar{\mathbf{G}}}_{e\,0}(\mathbf{r},\mathbf{r}')$ and $\bar{\bar{\mathbf{G}}}_{m\,0}(\mathbf{r},\mathbf{r}')$ [18]. The electric and magnetic fields $\mathbf{E}_n^1$ and $\mathbf{H}_n^1$ radiated by the exterior sources are computed by using the integral operator

$$\begin{bmatrix} \mathbf{E}_n^1(\mathbf{r}) \\ \mathbf{H}_n^1(\mathbf{r}) \end{bmatrix} = \begin{bmatrix} \iiint_{\mathbb{R}^3} \bar{\bar{\mathbf{G}}}_{e\,1}(\mathbf{r},\mathbf{r}') \cdot \mathbf{I}_n^0(\mathbf{r}')\mathrm{d}\mathbf{r}' \\ \iiint_{\mathbb{R}^3} \bar{\bar{\mathbf{G}}}_{m\,1}(\mathbf{r},\mathbf{r}') \cdot \mathbf{I}_n^0(\mathbf{r}')\mathrm{d}\mathbf{r}' \end{bmatrix} \tag{7}$$

with kernel the dyadic electric and magnetic Green's function $\bar{\bar{\mathbf{G}}}_{e\,1}(\mathbf{r},\mathbf{r}')$ and $\bar{\bar{\mathbf{G}}}_{m\,1}(\mathbf{r},\mathbf{r}')$ of the homogeneous space with dielectric permittivity $\varepsilon_1 = \varepsilon_0\varepsilon_r$ [18]. The integration is performed in both cases over the entire 3D space. The radiated electric and magnetic fields at an arbitrary point (ρ, φ, z) are computed by expanding the dyadic electric and magnetic Green's functions into cylindrical vector wave functions [18] and integrating.

Now, the MAS square linear system is constructed with respect to the unknown AS weights A_n, B_n, C_n, D_n by imposing the boundary conditions (continuity of the z and φ components of the total electric and magnetic fields) at N collocation points (CPs) on a cross section of the scatterer's surface

$$\begin{aligned}
&\sum_{n=1}^{N} E_{nz}^0(b,\phi_m,z) - \sum_{n=1}^{N} E_{nz}^1(b,\phi_m,z) \\
&\quad = -E_z^{\mathrm{inc}}(b,\phi_m,z) \qquad (m = 1,\dots N) \\
&\sum_{n=1}^{N} E_{n\phi}^0(b,\phi_m,z) - \sum_{n=1}^{N} E_{n\phi}^1(b,\phi_m,z) \\
&\quad = -E_\phi^{\mathrm{inc}}(b,\phi_m,z) \qquad (m = 1,\dots N) \\
&\sum_{n=1}^{N} H_{n\phi}^0(b,\phi_m,z) - \sum_{n=1}^{N} H_{n\phi}^1(b,\phi_m,z) \\
&\quad = -H_\phi^{\mathrm{inc}}(b,\phi_m,z) \qquad (m = 1,\dots,N) \\
&\sum_{n=1}^{N} H_{nz}^0(b,\phi_m,z) - \sum_{n=1}^{N} H_{nz}^1(b,\phi_m,z) = 0 \quad (m = 1,\dots N)
\end{aligned} \tag{8}$$

The linear system can be written in compact, block matrix form, as:

$$\begin{bmatrix} \mathbf{E}^{\mathbf{0}}_{\hat{\boldsymbol{\varphi}}\,\hat{\boldsymbol{\varphi}}} & \mathbf{E}^{\mathbf{0}}_{\hat{\boldsymbol{\varphi}}\hat{\mathbf{z}}} & \mathbf{E}^{\mathbf{1}}_{\hat{\boldsymbol{\varphi}}\,\hat{\boldsymbol{\varphi}}} & \mathbf{E}^{\mathbf{1}}_{\hat{\boldsymbol{\varphi}}\hat{\mathbf{z}}} \\ \mathbf{E}^{\mathbf{0}}_{\hat{\mathbf{z}}\hat{\boldsymbol{\varphi}}} & \mathbf{E}^{\mathbf{0}}_{\hat{\mathbf{z}}\hat{\mathbf{z}}} & \mathbf{E}^{\mathbf{1}}_{\hat{\mathbf{z}}\hat{\boldsymbol{\varphi}}} & \mathbf{E}^{\mathbf{1}}_{\hat{\mathbf{z}}\hat{\mathbf{z}}} \\ \mathbf{H}^{\mathbf{0}}_{\hat{\boldsymbol{\varphi}}\,\hat{\boldsymbol{\varphi}}} & \mathbf{H}^{\mathbf{0}}_{\hat{\boldsymbol{\varphi}}\hat{\mathbf{z}}} & \mathbf{H}^{\mathbf{1}}_{\hat{\boldsymbol{\varphi}}\,\hat{\boldsymbol{\varphi}}} & \mathbf{H}^{\mathbf{1}}_{\hat{\boldsymbol{\varphi}}\hat{\mathbf{z}}} \\ \mathbf{H}^{\mathbf{0}}_{\hat{\mathbf{z}}\hat{\boldsymbol{\varphi}}} & \mathbf{0} & \mathbf{H}^{\mathbf{1}}_{\hat{\mathbf{z}}\hat{\boldsymbol{\varphi}}} & \mathbf{0} \end{bmatrix} \begin{bmatrix} \mathbf{A} \\ \mathbf{B} \\ -\mathbf{C} \\ -\mathbf{D} \end{bmatrix} = - \begin{bmatrix} \mathbf{E}^{\mathrm{inc}}_{\boldsymbol{\varphi}} \\ \mathbf{E}^{\mathrm{inc}}_{\mathbf{z}} \\ \mathbf{H}^{\mathrm{inc}}_{\boldsymbol{\varphi}} \\ \mathbf{0} \end{bmatrix} \tag{9}$$

The matrix of the system is a 4×4 block matrix of $N \times N$ complex matrices with

$$\begin{aligned}
\left[E^{0,1}_{\hat{\phi}\hat{\phi}}\right]_{mn} &\equiv -\frac{j}{4}\exp\{-jk_z z\} \\
&\quad \times \sum_{l=-\infty}^{\infty} \left[\dot{J}_l\left(k_{x0,1}\rho_<^{1,0}\right) \dot{H}_l^{(2)}\left(k_{x0,1}\rho_>^{1,0}\right) \right. \\
&\qquad + \frac{l^2 k_z^2}{k_{0,1}^2\, a_{1,0}\, b\, k_{x0,1}^2} J_l\left(k_{x0,1}\rho_<^{1,0}\right) \\
&\qquad \left. \times H_l^{(2)}\left(k_{x0,1}\rho_>^{1,0}\right) \right] \exp\{jl(\phi_m - \phi_n)\} \\
\left[E^{0,1}_{\hat{\phi}\hat{z}}\right]_{mn} &\equiv -\frac{j}{4}\exp\{-jk_z z\} \\
&\quad \times \sum_{l=-\infty}^{\infty} \left[\frac{lk_z}{k_{0,1}^2\, b} J_l\left(k_{x0,1}\rho_<^{1,0}\right) H_l^{(2)}\left(k_{x0,1}\rho_>^{1,0}\right) \right] \\
&\quad \times \exp\{jl(\phi_m - \phi_n)\} \\
\left[E^{0,1}_{\hat{z}\hat{\phi}}\right]_{mn} &\equiv -\frac{j}{4}\exp\{-jk_z z\} \\
&\quad \times \sum_{l=-\infty}^{\infty} \left[\frac{lk_z}{k_{0,1}^2\, a_{1,0}} J_l\left(k_{x0,1}\rho_<^{1,0}\right) H_l^{(2)}\left(k_{x0,1}\rho_>^{1,0}\right) \right] \\
&\quad \times \exp\{jl(\phi_m - \phi_n)\} \\
\left[E^{0,1}_{\hat{z}\hat{z}}\right]_{mn} &\equiv -\frac{j}{4}\exp\{-jk_z z\} \\
&\quad \times \sum_{l=-\infty}^{\infty} \left[\frac{k_{x0,1}^2}{k_{0,1}^2} J_l\left(k_{x0,1}\rho_<^{1,0}\right) H_l^{(2)}\left(k_{x0,1}\rho_>^{1,0}\right) \right] \\
&\quad \times \exp\{jl(\phi_m - \phi_n)\} \\
\left[H^{0,1}_{\hat{\phi}\hat{\phi}}\right]_{mn} &\equiv -\frac{1}{4\omega\mu_0}\exp\{-jk_z z\} \\
&\quad \times \sum_{l=-\infty}^{\infty} \frac{lk_z}{k_{x0,1}} \left[\frac{1}{\rho_>^{1,0}} \dot{J}_l\left(k_{x0,1}\rho_<^{1,0}\right) H_l^{(2)}\left(k_{x0,1}\rho_>^{1,0}\right) \right. \\
&\qquad \left. + \frac{1}{\rho_<^{1,0}} J_l\left(k_{x0,1}\rho_<^{1,0}\right) \dot{H}_l^{(2)}\left(k_{x0,1}\rho_>^{1,0}\right) \right] \\
&\quad \times \exp\{jl(\phi_m - \phi_n)\}
\end{aligned}$$

$$\left[H^{1}_{\hat{\phi}\hat{z}}\right]_{mn} \equiv -\frac{1}{4\omega\mu_0}\exp\{-jk_z z\}\sum_{l=-\infty}^{\infty} k_{x1}\dot{J}_l\left(k_{x1}\rho^0_<\right)H^{(2)}_l \times\left(k_{x1}\rho^0_>\right)\exp\{jl(\phi_m-\phi_n)\}$$

$$\left[H^{0}_{\hat{\phi}\hat{z}}\right]_{mn} \equiv -\frac{1}{4\omega\mu_0}\exp\{-jk_z z\}\sum_{l=-\infty}^{\infty} k_{x0}J_l\left(k_{x0}\rho^1_<\right)\dot{H}^{(2)}_l \times\left(k_{x0}\rho^1_>\right)\exp\{jl(\phi_m-\phi_n)\}$$

$$\left[H^{1}_{\hat{z}\hat{\phi}}\right]_{mn} \equiv -\frac{1}{4\omega\mu_0}\exp\{-jk_z z\}\sum_{l=-\infty}^{\infty} k_{x1}J_l\left(k_{x1}\rho^0_<\right)\dot{H}^{(2)}_l \times\left(k_{x1}\rho^0_>\right)\exp\{jl(\phi_m-\phi_n)\}$$

$$\left[H^{0}_{\hat{z}\hat{\phi}}\right]_{mn} \equiv -\frac{1}{4\omega\mu_0}\exp\{-jk_z z\}\sum_{l=-\infty}^{\infty} k_{x0}\,\dot{J}_l\left(k_{x0}\rho^1_<\right)H^{(2)}_l \times\left(k_{x0}\rho^1_>\right)\exp\{jl(\phi_m-\phi_n)\}$$

$$\left[H^{0,1}_{\hat{z}\hat{z}}\right]_{mn} \equiv 0 \tag{10}$$

where $J_l(x)$ and $H^{(2)}_l(x)$ are the cylindrical Bessel and Hankel functions of order l, the dot denotes derivation with respect to the entire argument, $\rho^{0,1}_< \equiv \min(a_{0,1}, b)$, $\rho^{0,1}_> \equiv \max(a_{0,1}, b)$, $k_{x0,1} = \sqrt{k^2_{0,1} - k^2_z}$ and $k_1 = k_0\sqrt{\varepsilon_r}$. Furthermore, **A**, **B**,**C**, **D** are $N \times 1$ column vectors containing the unknown AS weights A_n, B_n, C_n, D_n, and $\mathbf{E}^{\text{inc}}_{\boldsymbol{\varphi}}$, $\mathbf{E}^{\text{inc}}_{\mathbf{z}}$, $\mathbf{H}^{\text{inc}}_{\boldsymbol{\varphi}}$ are $N \times 1$ column vectors consisting of the incident field's components sampled at the N CPs. It is interesting to note that when $k_z = 0(\theta_i = 90°)$ the matrix elements given by (10) coincide with the corresponding ones of the normal incidence problem derived in [13].

The study of the MAS accuracy is based on the analytic inversion of (9). A technique similar to that of [11] and [19] can be invoked for the diagonalization of each block, which will result in the inversion of the MAS matrix. Since each block of the MAS matrix is a circulant matrix, the eigenvalues and corresponding eigenvectors have explicit expressions [20], which yield

$$\mathbf{F} = \mathbf{G}\,\mathbf{D_F}\,\mathbf{G}^{-1} \tag{11}$$

where **F** represents any of the sixteen blocks of the MAS matrix, $\mathbf{D_F}$ is a diagonal matrix containing the eigenvalues of **F**, which are respectively given by ($q = 1, \ldots, N$)

$$\left[D_{E^{0,1}_{\hat{\phi}\hat{\phi}}}\right]_q \equiv -\frac{jN}{4}\exp\{-jk_z z\} \times\sum_{s=-\infty}^{\infty}\left[\dot{J}_{q+sN}\left(k_{x0,1}\rho^{1,0}_<\right)\dot{H}^{(2)}_{q+sN}\left(k_{x0,1}\rho^{1,0}_>\right) + \frac{(q+sN)^2k_z^2}{k^2_{0,1}\,a_{1,0}\,b\,k^2_{x0,1}}J_{q+sN}\left(k_{x0,1}\rho^{1,0}_<\right) \times H^{(2)}_{q+sN}\left(k_{x0,1}\rho^{1,0}_>\right)\right]$$

$$\left[D_{E^{0,1}_{\hat{\phi}\hat{z}}}\right]_q \equiv -\frac{jN}{4}\exp\{-jk_z z\} \times\sum_{s=-\infty}^{\infty}\left[\frac{(q+sN)k_z}{k^2_{0,1}\,b}J_{q+sN}\left(k_{x0,1}\rho^{1,0}_<\right)H^{(2)}_{q+sN} \times\left(k_{x0,1}\rho^{1,0}_>\right)\right]$$

$$\left[D_{E^{0,1}_{\hat{z}\hat{\phi}}}\right]_q \equiv -\frac{jN}{4}\exp\{-jk_z z\} \times\sum_{s=-\infty}^{\infty}\left[\frac{(q+sN)k_z}{k^2_{0,1}\,a_{1,0}}J_{q+sN}\left(k_{x0,1}\rho^{1,0}_<\right)H^{(2)}_{q+sN} \times\left(k_{x0,1}\rho^{1,0}_>\right)\right]$$

$$\left[D_{E^{0,1}_{\hat{z}\hat{z}}}\right]_q \equiv -\frac{jN}{4}\exp\{-jk_z z\} \times\sum_{s=-\infty}^{\infty}\left[\frac{k^2_{x0,1}}{k^2_{0,1}}J_{q+sN}\left(k_{x0,1}\rho^{1,0}_<\right)H^{(2)}_{q+sN} \times\left(k_{x0,1}\rho^{1,0}_>\right)\right]$$

$$\left[D_{H^{0,1}_{\hat{\phi}\hat{\phi}}}\right]_q \equiv -\frac{N}{4\omega\mu_0}\exp\{-jk_z z\}\sum_{s=-\infty}^{\infty}\frac{(q+sN)k_z}{k_{x0,1}} \times\left[\frac{1}{\rho^{1,0}_>}\dot{J}_{q+sN}\left(k_{x0,1}\rho^{1,0}_<\right)H^{(2)}_{q+sN}\left(k_{x0,1}\rho^{1,0}_>\right) + \frac{1}{\rho^{1,0}_<}J_{q+sN}\left(k_{x0,1}\rho^{1,0}_<\right)\dot{H}^{(2)}_{q+sN}\left(k_{x0,1}\rho^{1,0}_>\right)\right]$$

$$\left[D_{H^{1}_{\hat{\phi}\hat{z}}}\right]_q \equiv -\frac{N}{4\omega\mu_0}\exp\{-jk_z z\} \times\sum_{s=-\infty}^{\infty}\left[k_{x1}\dot{J}_{q+sN}\left(k_{x1}\rho^0_<\right)H^{(2)}_{q+sN}\left(k_{x1}\rho^0_>\right)\right]$$

$$\left[D_{H^{0}_{\hat{\phi}\hat{z}}}\right]_q \equiv -\frac{N}{4\omega\mu_0}\exp\{-jk_z z\} \times\sum_{s=-\infty}^{\infty}\left[k_{x0}J_{q+sN}\left(k_{x0}\rho^1_<\right)\dot{H}^{(2)}_{q+sN}\left(k_{x0}\rho^1_>\right)\right]$$

$$\left[D_{H^{1}_{\hat{z}\hat{\phi}}}\right]_q \equiv -\frac{N}{4\omega\mu_0}\exp\{-jk_z z\} \times\sum_{s=-\infty}^{\infty}\left[k_{x1}J_{q+sN}\left(k_{x1}\rho^0_<\right)\dot{H}^{(2)}_{q+sN}\left(k_{x1}\rho^0_>\right)\right]$$

$$\left[D_{H^{0}_{\hat{z}\hat{\phi}}}\right]_q \equiv -\frac{N}{4\omega\mu_0}\exp\{-jk_z z\} \times\sum_{s=-\infty}^{\infty}\left[k_{x0}\,\dot{J}_{q+sN}\left(k_{x0}\rho^1_<\right)H^{(2)}_{q+sN}\left(k_{x0}\rho^1_>\right)\right], \tag{12}$$

and **G** is the eigenvector square matrix, which is common for all blocks **F**. The eigenvector matrix is identical to the case of oblique incidence on a perfectly conducting cylinder [11], because there the MAS matrix is also composed of circulant blocks.

Now, by using (9) and (11), we obtain the diagonalization of the MAS matrix

$$\begin{aligned}\mathbf{Z} &= \begin{bmatrix} \mathbf{E}^0_{\hat\varphi\hat\varphi} & \mathbf{E}^0_{\hat\varphi\hat z} & \mathbf{E}^1_{\hat\varphi\hat\varphi} & \mathbf{E}^1_{\hat\varphi\hat z} \\ \mathbf{E}^0_{\hat z\hat\varphi} & \mathbf{E}^0_{\hat z\hat z} & \mathbf{E}^1_{\hat z\hat\varphi} & \mathbf{E}^1_{\hat z\hat z} \\ \mathbf{H}^0_{\hat\varphi\hat\varphi} & \mathbf{H}^0_{\hat\varphi\hat z} & \mathbf{H}^1_{\hat\varphi\hat\varphi} & \mathbf{H}^1_{\hat\varphi\hat z} \\ \mathbf{H}^0_{\hat z\hat\varphi} & \mathbf{0} & \mathbf{H}^1_{\hat z\hat\varphi} & \mathbf{0} \end{bmatrix} \\ &= \begin{bmatrix} \mathbf{G} & \mathbf{0} & \mathbf{0} & \mathbf{0} \\ \mathbf{0} & \mathbf{G} & \mathbf{0} & \mathbf{0} \\ \mathbf{0} & \mathbf{0} & \mathbf{G} & \mathbf{0} \\ \mathbf{0} & \mathbf{0} & \mathbf{0} & \mathbf{G} \end{bmatrix} \begin{bmatrix} \mathbf{D}_{\mathbf{E}^0_{\hat\varphi\hat\varphi}} & \mathbf{D}_{\mathbf{E}^0_{\hat\varphi\hat z}} & \mathbf{D}_{\mathbf{E}^1_{\hat\varphi\hat\varphi}} & \mathbf{D}_{\mathbf{E}^1_{\hat\varphi\hat z}} \\ \mathbf{D}_{\mathbf{E}^0_{\hat z\hat\varphi}} & \mathbf{D}_{\mathbf{E}^0_{\hat z\hat z}} & \mathbf{D}_{\mathbf{E}^1_{\hat z\hat\varphi}} & \mathbf{D}_{\mathbf{E}^1_{\hat z\hat z}} \\ \mathbf{D}_{\mathbf{H}^0_{\hat\varphi\hat\varphi}} & \mathbf{D}_{\mathbf{H}^0_{\hat\varphi\hat z}} & \mathbf{D}_{\mathbf{H}^1_{\hat\varphi\hat\varphi}} & \mathbf{D}_{\mathbf{H}^1_{\hat\varphi\hat z}} \\ \mathbf{D}_{\mathbf{H}^0_{\hat z\hat\varphi}} & \mathbf{0} & \mathbf{D}_{\mathbf{H}^1_{\hat z\hat\varphi}} & \mathbf{0} \end{bmatrix} \\ &\quad \times \begin{bmatrix} \mathbf{G}^{-1} & \mathbf{0} & \mathbf{0} & \mathbf{0} \\ \mathbf{0} & \mathbf{G}^{-1} & \mathbf{0} & \mathbf{0} \\ \mathbf{0} & \mathbf{0} & \mathbf{G}^{-1} & \mathbf{0} \\ \mathbf{0} & \mathbf{0} & \mathbf{0} & \mathbf{G}^{-1} \end{bmatrix} \end{aligned} \tag{13}$$

where $\mathbf{0}$ is the $N \times N$ null matrix. Thus, the analytic inversion of **Z** is reduced to the analytic inversion of the $4N \times 4N$ matrix

$$\mathbf{D} = \begin{bmatrix} \mathbf{D}_{\mathbf{E}^0_{\hat\varphi\hat\varphi}} & \mathbf{D}_{\mathbf{E}^0_{\hat\varphi\hat z}} & \mathbf{D}_{\mathbf{E}^1_{\hat\varphi\hat\varphi}} & \mathbf{D}_{\mathbf{E}^1_{\hat\varphi\hat z}} \\ \mathbf{D}_{\mathbf{E}^0_{\hat z\hat\varphi}} & \mathbf{D}_{\mathbf{E}^0_{\hat z\hat z}} & \mathbf{D}_{\mathbf{E}^1_{\hat z\hat\varphi}} & \mathbf{D}_{\mathbf{E}^1_{\hat z\hat z}} \\ \mathbf{D}_{\mathbf{H}^0_{\hat\varphi\hat\varphi}} & \mathbf{D}_{\mathbf{H}^0_{\hat\varphi\hat z}} & \mathbf{D}_{\mathbf{H}^1_{\hat\varphi\hat\varphi}} & \mathbf{D}_{\mathbf{H}^1_{\hat\varphi\hat z}} \\ \mathbf{D}_{\mathbf{H}^0_{\hat z\hat\varphi}} & \mathbf{0} & \mathbf{D}_{\mathbf{H}^1_{\hat z\hat\varphi}} & \mathbf{0} \end{bmatrix} \tag{14}$$

Now by successive use of the matrix identity

$$\begin{aligned}&\begin{bmatrix} \mathbf{X} & \mathbf{Y} \\ \mathbf{Z} & \mathbf{W} \end{bmatrix}^{-1} \\ &= \begin{bmatrix} -\mathbf{Z}^{-1}\mathbf{W}(\mathbf{I}-\mathbf{Y}^{-1}\mathbf{X}\mathbf{Z}^{-1}\mathbf{W})^{-1}\mathbf{Y}^{-1} & (\mathbf{I}-\mathbf{Z}^{-1}\mathbf{W}\mathbf{Y}^{-1}\mathbf{X})^{-1}\mathbf{Z}^{-1} \\ (\mathbf{I}-\mathbf{Y}^{-1}\mathbf{X}\mathbf{Z}^{-1}\mathbf{W})^{-1}\mathbf{Y}^{-1} & -\mathbf{Y}^{-1}\mathbf{X}(\mathbf{I}-\mathbf{Z}^{-1}\mathbf{W}\mathbf{Y}^{-1}\mathbf{X})^{-1}\mathbf{Z}^{-1} \end{bmatrix},\end{aligned} \tag{15}$$

which holds if all the inversions appearing on the right hand side are feasible, we describe in two steps an analytic method for the inversion of **D**.

Step 1: We split **D** into four 2×2 block matrices

$$\mathbf{D} = \begin{bmatrix} \mathbf{X} & \mathbf{Y} \\ \mathbf{Z} & \mathbf{W} \end{bmatrix} \tag{16}$$

where

$$\mathbf{X} = \begin{bmatrix} \mathbf{D}_{\mathbf{E}^0_{\hat\varphi\hat\varphi}} & \mathbf{D}_{\mathbf{E}^0_{\hat\varphi\hat z}} \\ \mathbf{D}_{\mathbf{E}^0_{\hat z\hat\varphi}} & \mathbf{D}_{\mathbf{E}^0_{\hat z\hat z}} \end{bmatrix} \quad \mathbf{Y} = \begin{bmatrix} \mathbf{D}_{\mathbf{E}^1_{\hat\varphi\hat\varphi}} & \mathbf{D}_{\mathbf{E}^1_{\hat\varphi\hat z}} \\ \mathbf{D}_{\mathbf{E}^1_{\hat z\hat\varphi}} & \mathbf{D}_{\mathbf{E}^1_{\hat z\hat z}} \end{bmatrix}$$

$$\mathbf{Z} = \begin{bmatrix} \mathbf{D}_{\mathbf{H}^0_{\hat\varphi\hat\varphi}} & \mathbf{D}_{\mathbf{H}^0_{\hat\varphi\hat z}} \\ \mathbf{D}_{\mathbf{H}^0_{\hat z\hat\varphi}} & \mathbf{0} \end{bmatrix} \quad \mathbf{W} = \begin{bmatrix} \mathbf{D}_{\mathbf{H}^1_{\hat\varphi\hat\varphi}} & \mathbf{D}_{\mathbf{H}^1_{\hat\varphi\hat z}} \\ \mathbf{D}_{\mathbf{H}^1_{\hat z\hat\varphi}} & \mathbf{0} \end{bmatrix}$$

By taking into account (14) and (15), we conclude that the inversion of the 4×4 block matrix **D** is reduced to the inversions of the 2×2 block matrices **Y**, **Z**, $(\mathbf{I}-\mathbf{Y}^{-1}\mathbf{X}\mathbf{Z}^{-1}\mathbf{W})$, $(\mathbf{I}-\mathbf{Z}^{-1}\mathbf{W}\mathbf{Y}^{-1}\mathbf{X})$. Hence, the inversion of the original matrix **D** is obtained by inverting matrices with half dimension.

Step 2: Here, we have to invert 2×2 block diagonal matrices, whose inversion is obtained by using the following matrix identity

$$\begin{aligned}\begin{bmatrix} \mathbf{X} & \mathbf{Y} \\ \mathbf{Z} & \mathbf{W} \end{bmatrix}^{-1} &= \begin{bmatrix} \mathbf{W} & -\mathbf{Y} \\ -\mathbf{Z} & \mathbf{X} \end{bmatrix} \\ &\quad \times \begin{bmatrix} (\mathbf{X}\mathbf{W}-\mathbf{Y}\mathbf{Z})^{-1} & \mathbf{0} \\ \mathbf{0} & (\mathbf{X}\mathbf{W}-\mathbf{Y}\mathbf{Z})^{-1} \end{bmatrix}\end{aligned} \tag{17}$$

which holds if and only if the matrices commute in pairs, and is therefore applicable to diagonal blocks.

3 Analytic error estimation

The above analysis is utilized to express analytically the boundary condition error at the midpoints (MPs) between each two successive CPs. The MPs are defined by the azimuth angles $\phi = \phi_m + \tilde\phi$, $1 \le m \le N$, where $\tilde\phi \equiv \pi/N$ and $\phi_m \equiv m(2\pi/N)$ is the azimuth angle of the mth CP. By following techniques similar to [11] and [13], we express the tangential components of the electric fields radiated by the ASs at the MPs

$$\begin{bmatrix} \tilde{\mathbf{E}}^{\mathrm{rad}}_{\varphi} \\ \tilde{\mathbf{E}}^{\mathrm{rad}}_{z} \\ \tilde{\mathbf{H}}^{\mathrm{rad}}_{\varphi} \\ \tilde{\mathbf{H}}^{\mathrm{rad}}_{z} \end{bmatrix} = \begin{bmatrix} \tilde{\mathbf{E}}^0_{\hat\varphi\hat\varphi} & \tilde{\mathbf{E}}^0_{\hat\varphi\hat z} & \tilde{\mathbf{E}}^1_{\hat\varphi\hat\varphi} & \tilde{\mathbf{E}}^1_{\hat\varphi\hat z} \\ \tilde{\mathbf{E}}^0_{\hat z\hat\varphi} & \tilde{\mathbf{E}}^0_{\hat z\hat z} & \tilde{\mathbf{E}}^1_{\hat z\hat\varphi} & \tilde{\mathbf{E}}^1_{\hat z\hat z} \\ \tilde{\mathbf{H}}^0_{\hat\varphi\hat\varphi} & \tilde{\mathbf{H}}^0_{\hat\varphi\hat z} & \tilde{\mathbf{H}}^1_{\hat\varphi\hat\varphi} & \tilde{\mathbf{H}}^1_{\hat\varphi\hat z} \\ \tilde{\mathbf{H}}^0_{\hat z\hat\varphi} & \mathbf{0} & \tilde{\mathbf{H}}^1_{\hat z\hat\varphi} & \mathbf{0} \end{bmatrix} \begin{bmatrix} \mathbf{A} \\ \mathbf{B} \\ -\mathbf{C} \\ -\mathbf{D} \end{bmatrix} \tag{18}$$

where the symbol ∼ above each variable denotes the corresponding quantity evaluated at the MPs. Furthermore we have

$$\tilde{\mathbf{F}} = \mathbf{G}\,\mathbf{D}_{\tilde{\mathbf{F}}}\mathbf{G}^{-1} \tag{19}$$

where $\tilde{\mathbf{F}}$ represents any of the sixteen blocks of the matrix in (18) and $\mathbf{D}_{\tilde{\mathbf{F}}}$ is a diagonal matrix containing the eigenvalues of $\tilde{\mathbf{F}}$, which are respectively given by ($q = 1, \ldots, N$)

$$\left[D_{\tilde{E}^{0,1}_{\hat{\phi}\hat{\phi}}}\right]_q \equiv -\frac{jN}{4}\exp\{-jk_z z\}\sum_{s=-\infty}^{\infty}\left[\dot{J}_{q+sN}\left(k_{x0,1}\rho_<^{1,0}\right)\dot{H}^{(2)}_{q+sN}\left(k_{x0,1}\rho_>^{1,0}\right)+\frac{(q+sN)^2k_z^2}{k_{0,1}^2\,a_{1,0}\,b\,k_{x0,1}^2}J_{q+sN}\left(k_{x0,1}\rho_<^{1,0}\right)\right.$$
$$\left.\times H^{(2)}_{q+sN}\left(k_{x0,1}\rho_>^{1,0}\right)\right]\exp\{j(q+sN)\tilde{\phi}\}$$

$$\left[D_{\tilde{E}^{0,1}_{\hat{\phi}\hat{z}}}\right]_q \equiv -\frac{jN}{4}\exp\{-jk_z z\}\sum_{s=-\infty}^{\infty}\left[\frac{(q+sN)k_z}{k_{0,1}^2\,b}J_{q+sN}\left(k_{x0,1}\rho_<^{1,0}\right)H^{(2)}_{q+sN}\left(k_{x0,1}\rho_>^{1,0}\right)\right]\exp\{j(q+sN)\tilde{\phi}\}$$

$$\left[D_{\tilde{E}^{0,1}_{\hat{z}\hat{\phi}}}\right]_q \equiv -\frac{jN}{4}\exp\{-jk_z z\}\sum_{s=-\infty}^{\infty}\left[\frac{(q+sN)k_z}{k_{0,1}^2\,a_{1,0}}J_{q+sN}\left(k_{x0,1}\rho_<^{1,0}\right)H^{(2)}_{q+sN}\left(k_{x0,1}\rho_>^{1,0}\right)\right]\exp\{j(q+sN)\tilde{\phi}\}$$

$$\left[D_{\tilde{E}^{0,1}_{\hat{z}\hat{z}}}\right]_q \equiv -\frac{jN}{4}\exp\{-jk_z z\}\sum_{s=-\infty}^{\infty}\left[\frac{k_{x0,1}^2}{k_{0,1}^2}J_{q+sN}\left(k_{x0,1}\rho_<^{1,0}\right)H^{(2)}_{q+sN}\left(k_{x0,1}\rho_>^{1,0}\right)\right]\exp\{j(q+sN)\tilde{\phi}\}$$

$$\left[D_{\tilde{H}^{0,1}_{\hat{\phi}\hat{\phi}}}\right]_q \equiv -\frac{N}{4\omega\mu_0}\exp\{-jk_z z\}\sum_{s=-\infty}^{\infty}\frac{(q+sN)k_z}{k_{x0,1}}\left[\frac{1}{\rho_>^{1,0}}\dot{J}_{q+sN}\left(k_{x0,1}\rho_<^{1,0}\right)H^{(2)}_{q+sN}\left(k_{x0,1}\rho_>^{1,0}\right)\right.$$
$$\left.+\frac{1}{\rho_<^{1,0}}J_{q+sN}\left(k_{x0,1}\rho_<^{1,0}\right)\dot{H}^{(2)}_{q+sN}\left(k_{x0,1}\rho_>^{1,0}\right)\right]\exp\{j(q+sN)\tilde{\phi}\}$$

$$\left[D_{\tilde{H}^{1}_{\hat{\phi}\hat{z}}}\right]_q \equiv -\frac{N}{4\omega\mu_0}\exp\{-jk_z z\}\sum_{s=-\infty}^{\infty}\left[k_{x1}\dot{J}_{q+sN}\left(k_{x1}\rho_<^{0}\right)H^{(2)}_{q+sN}\left(k_{x1}\rho_>^{0}\right)\right]\exp\{j(q+sN)\tilde{\phi}\}$$

$$\left[D_{\tilde{H}^{0}_{\hat{\phi}\hat{z}}}\right]_q \equiv -\frac{N}{4\omega\mu_0}\exp\{-jk_z z\}\sum_{s=-\infty}^{\infty}\left[k_{x0}J_{q+sN}\left(k_{x0}\rho_<^{1}\right)\dot{H}^{(2)}_{q+sN}\left(k_{x0}\rho_>^{1}\right)\right]\exp\{j(q+sN)\tilde{\phi}\}$$

$$\left[D_{\tilde{H}^{1}_{\hat{z}\hat{\phi}}}\right]_q \equiv -\frac{N}{4\omega\mu_0}\exp\{-jk_z z\}\sum_{s=-\infty}^{\infty}\left[k_{x1}J_{q+sN}\left(k_{x1}\rho_<^{0}\right)\dot{H}^{(2)}_{q+sN}\left(k_{x1}\rho_>^{0}\right)\right]\exp\{j(q+sN)\tilde{\phi}\}$$

$$\left[D_{\tilde{H}^{0}_{\hat{z}\hat{\phi}}}\right]_q \equiv -\frac{N}{4\omega\mu_0}\exp\{-jk_z z\}\sum_{s=-\infty}^{\infty}\left[k_{x0}\,\dot{J}_{q+sN}\left(k_{x0}\rho_<^{1}\right)H^{(2)}_{q+sN}\left(k_{x0}\rho_>^{1}\right)\right]\exp\{j(q+sN)\tilde{\phi}\} \tag{20}$$

The accuracy of the method at the MPs is validated by the mean square residual error in the boundary condition

$$e(a_0,a_1,b,N)=\frac{\left\|\begin{bmatrix}\tilde{\mathbf{E}}^{\mathbf{rad}}_{\boldsymbol{\varphi}}\\ \tilde{\mathbf{E}}^{\mathbf{rad}}_{\mathbf{z}}\\ \tilde{\mathbf{H}}^{\mathbf{rad}}_{\boldsymbol{\varphi}}Z_0\\ \tilde{\mathbf{H}}^{\mathbf{rad}}_{\mathbf{z}}Z_0\end{bmatrix}+\begin{bmatrix}\tilde{\mathbf{E}}^{\mathbf{inc}}_{\boldsymbol{\varphi}}\\ \tilde{\mathbf{E}}^{\mathbf{inc}}_{\mathbf{z}}\\ \tilde{\mathbf{H}}^{\mathbf{inc}}_{\boldsymbol{\varphi}}Z_0\\ \mathbf{0}\end{bmatrix}\right\|_2}{\left\|\begin{bmatrix}\tilde{\mathbf{E}}^{\mathbf{inc}}_{\boldsymbol{\varphi}}\\ \tilde{\mathbf{E}}^{\mathbf{inc}}_{\mathbf{z}}\\ \tilde{\mathbf{H}}^{\mathbf{inc}}_{\boldsymbol{\varphi}}Z_0\\ \mathbf{0}\end{bmatrix}\right\|_2} \tag{21}$$

where $\tilde{\mathbf{E}}^{\mathbf{inc}}_{\boldsymbol{\varphi}}$, $\tilde{\mathbf{E}}^{\mathbf{inc}}_{z}$, $\tilde{\mathbf{H}}^{\mathbf{inc}}_{\phi}$ are the incident fields' components evaluated at the MPs, and $||.||_2$ is the standard 2-norm. Thus, the highest possible accuracy for the MAS solution is achieved by minimizing e in (21) for appropriate a_0 and a_1 for given b, N, θ_i and ε_r.

4 Numerical results and discussion

The expressions derived in the previous sections are validated by examining several cases for various parameters. The analytical error is calculated by use of (21). The computational error is calculated by the LU decomposition and numerical inversion of the MAS matrix. Figs. 3 and 4 show the comparison between the analytical and the computational error with respect to a_1 for incidence angles $\theta_i = 45°, 70°$, respectively. Three sets of curves are plotted in each figure, for $N = 20$, 30 and 40. The vertical axis maps the base 10 logarithm of the error, while the horizontal axis maps the ratio a_1/b. Furthermore, the MAS matrix condition number is plotted in Fig. 5 for $\theta_i = 45°$ and $N = 20$, 30, 40, while for different incidence angles the behavior of the condition number remains almost identical.

It is worth noting that, for a wide range of radius a_1, the analytical and the computational error coincide, as expected. However, for small values of a_1 the analytical error

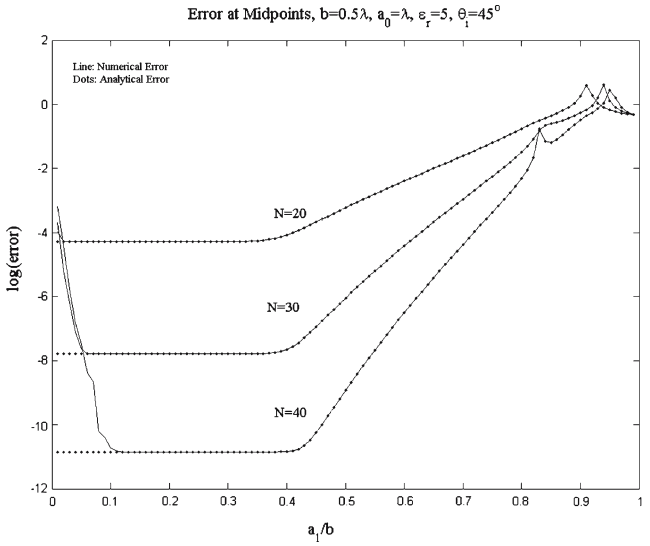

Fig. 3 Numerical and analytical midpoint error plots as a function of a_1/b for $b = 0.5\lambda$, $a_0 = \lambda$, $\varepsilon_r = 5$, $\theta_i = 45°$ and various numbers of unknowns N

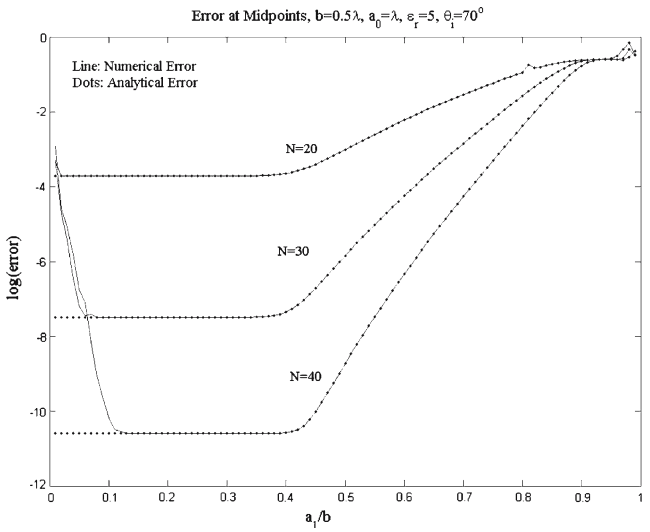

Fig. 4 Numerical and analytical midpoint error plots as a function of a_1/b for $b = 0.5\lambda$, $a_0 = \lambda$, $\varepsilon_r = 5$, $\theta_i = 70°$ and various numbers of unknowns N

remains bounded (and low), while the computational error demonstrates a highly irregular behavior. This discrepancy is due to the high values of the system's condition number in this range of a_1, which evidently affects the numerical error, but leaves the analytical error intact. Figure 5 indicates that the condition number grows steeper than exponentially when a_1 approaches 0. Moreover, the range of the erratic fluctuation increases with the number N of the ASs, which determines the dimension of the MAS matrix, an effect clearly inferred by the curves in Fig. 5. The curves of Figs. 3 and 5 show that the computational error succumbs to noise influence for condition numbers greater than 10^{16} (MATLAB implementation with double precision arithmetic).

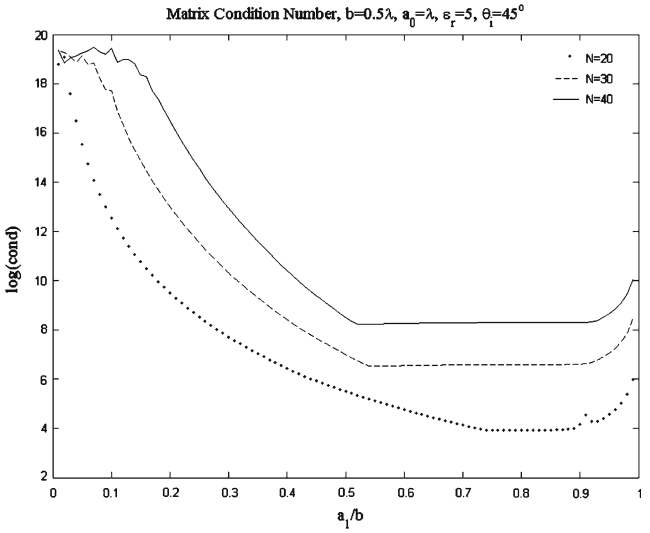

Fig. 5 MAS matrix condition number as a function of a_1/b for $b = 0.5\lambda$, $a_0 = \lambda$, $\varepsilon_r = 5$, $\theta_i = 45°$ and various numbers N of auxiliary sources

A different kind of disagreement appears when a_1 approaches b. In this case, the condition number remains sufficiently low (see Fig. 5), and hence it is not responsible for the problem. This situation is due to the fact that the diagonal elements in the blocks of the MAS matrix become unbounded, since the ASs and the CPs tend to coincide. The final outcome is that both types of errors, although unequal, attain excessively high levels when the fictitious surface approaches the actual boundary.

Furthermore, spike-like features appear in several locations for both the analytical and the computational errors. These peaks are associated with resonances, caused by vanishing denominators in the expression (21). As discussed in [11], the locations of these resonances are related to the roots of Bessel functions and their derivatives. From expression (15) it is evident that the resonances of the current problem are a superposition of the resonances inherited by the normal incidence problem [13] corresponding to the inversion of each block matrix $\mathbf{Y}$, $\mathbf{Z}$, and the resonances generated by the inversion of the terms $(\mathbf{I} - \mathbf{Y}^{-1}\mathbf{X}\mathbf{Z}^{-1}\mathbf{W})$ and $(\mathbf{I}-\mathbf{Z}^{-1}\mathbf{W}\mathbf{Y}^{-1}\mathbf{X})$. These terms express the coupling between the blocks of the MAS matrix and are present only in the oblique incidence problem.

To assess the dependence of the MAS accuracy on the location of the exterior ASs, Fig. 6 compares the analytical with the computational error as a function of a_0 for incidence angle $\theta_i = 70°$. It is concluded that the error is practically independent of the location of S^0, provided the outer auxiliary surface is sufficiently far from S. This result is also observed and discussed in the normal incidence case [13], where it is proven that there are no resonances associated with the location of S^0.

Finally, the effect of the dielectric permittivity on the error is shown in Fig. 7, where the logarithm of the error is plotted as a function of ε_r. Like in [13], the protrusions observed in Fig. 7 do not represent resonances [caused by vanishing

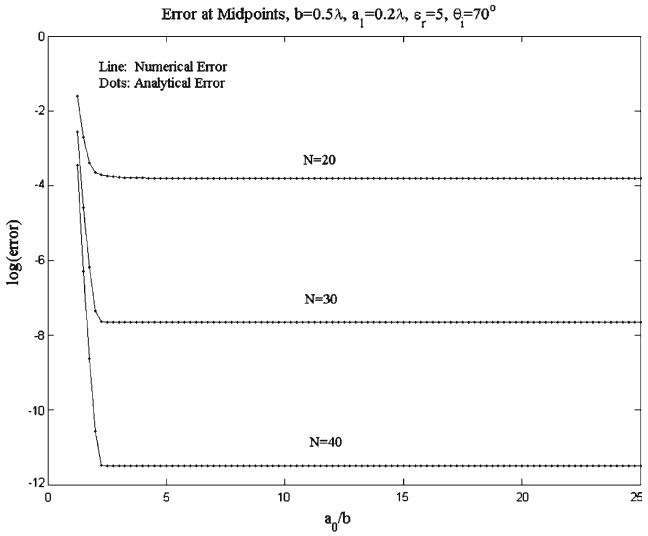

Fig. 6 Numerical and analytical midpoint error plots as a function of a_0/b for $b = 0.5\lambda$, $a_1 = 0.2\lambda$, $\varepsilon_r = 5$, $\theta_i = 70°$ and various numbers of unknowns N

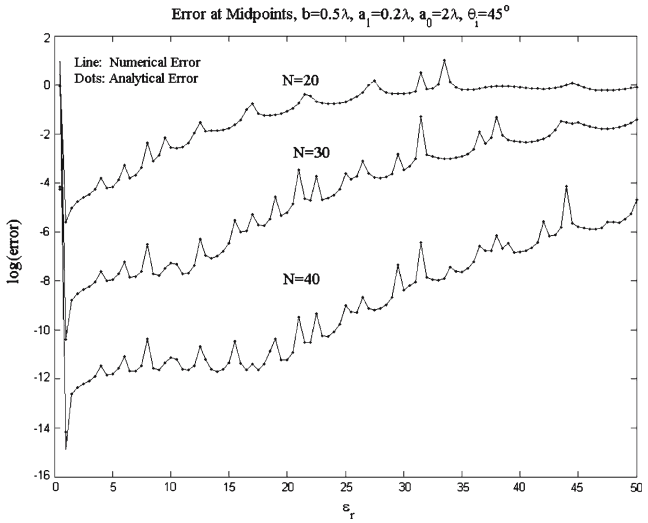

Fig. 7 Numerical and analytical midpoint error plots as a function of ε_r for $b = 0.5\lambda$, $a_1 = 0.2\lambda$, $a_0 = 2\lambda$, $\theta_i = 45°$ and various numbers of unknowns N

denominators in (21)], but are due to the rapidly oscillating behavior of the functions involved in the matrix blocks in (18).

By using the above analysis, we determine the range of the auxiliary surface radii, which yield the most accurate numerical solution. In particular, ratio a_1/b should be chosen as small as possible, provided that the condition number of the system does not exceed a certain upper bound. The arithmetic precision of the calculations determine the acceptable condition number levels. For our own implementation (MATLAB with double precision arithmetic) inner auxiliary surfaces radii, corresponding to a condition number higher than 10^{16} should be avoided. On the other hand, the MAS accuracy is independent of the ratio a_0/b, provided that the latter is not chosen too close to 1. Finally, regarding the particular incidence angle θ_i, it is necessary to examine which radii of the interior auxiliary surface generate resonances, in order that a_1 is not chosen in the vicinity of these radii.

5 Conclusions

The MAS accuracy for oblique incidence TM^z plane wave scattering from a dielectric, infinite, circular cylinder was fully investigated. The MAS linear system was inverted analytically, yielding exact expressions for the discretization error. Numerical results revealed smooth behavior of this error for a wide range of ASs radii, with the exception of a denumerable set of resonance locations. These locations were determined analytically as the ASs radii for which the MAS matrix becomes singular. On the other hand, the actual computational error, calculated through numerical matrix inversion, showed significant corruption due to numerical noise, for condition numbers exceeding a specific threshold, determined by the arithmetic precision of the calculations. The analytical error decreases with the number of the ASs, thus verifying the MAS theoretically guaranteed convergence to the exact solution. In practice, though, this convergence is not easily observable, due to poor conditioning, which introduces severe numerical instabilities. Finally, several criteria facilitating the optimal choice of the auxiliary surface location were explicitly stated, deduced from both the analytical and numerical results.

The analysis presented can be exploited for the application of MAS in more general geometries involving cylindrical symmetry. Specifically, the conclusions drawn in this paper about the optimal location of the ASs can be extended into scattering problems involving layered dielectric cylinders, a configuration which is quite intricate to simulate via standard techniques. Practical projections in the future may include direct and inverse scattering from vegetation, modelled as an array of inhomogeneous dielectric cylinders, with obvious applications in remote sensing. Also the analysis is very helpful in the simulation of embedded dielectric resonator cylindrical antennas, which often replace their perfect electric conductor counterparts at high frequencies when ohmic losses of the latter are prohibitive.

References

1. Kaklamani DI, Anastassiu HT (2002) Aspects of the method of auxiliary sources (MAS) in computational electromagnetics. IEEE Antennas Propagation Mag 44:48–64
2. Fairweather G, Karageorghis A, Martin PA (2003) The method of fundamental solutions for scattering and radiation problems. Eng Anal Bound Elem 27:759–769
3. Zaridze RS, Bit-Babik G, Tavzarashvili K, Economou DP, Uzunoglu NK (2002) Wave field singularity aspects in large-size scatterers and inverse problems. IEEE Trans Antennas Propagation 50:50–58
4. Leviatan Y (1990) Analytic continuation considerations when using generalized formulations for scattering problems. IEEE Trans Antennas Propagation 38:1259–1263

5. Doicu A, Eremin Yu, Wriedt T (2000) Acoustic and electromagnetic scattering analysis using discrete sources. Academic, New York
6. Leviatan Y, Boag A (1987) Analysis of electromagnetic scattering from dielectric cylinders using a multifilament current model. IEEE Trans Antennas Propagation 35:1119–1127
7. Anastassiu HT, Kaklamani DI, Economou DP, Breinbjerg O (2002) Electromagnetic scattering analysis of coated conductors with edges using the method of auxiliary sources (MAS) in conjunction with the standard impedance boundary condition, (SIBC). IEEE Trans Antennas Propagation 50:59–66
8. Avdikos GK, Anastassiu HT (2005) Computational cost estimations and comparisons for three methods of applied electromagnetics (MoM, MAS, MMAS). IEEE Antennas Propagation Mag 47:121–129
9. Anastassiu HT, Lymperopoulos DG, Kaklamani DI (2004) Accuracy analysis and optimization of the method of auxiliary sources (MAS) for scattering by a circular cylinder. IEEE Trans Antennas Propagation 52:1541–1547
10. Anastassiu HT, Kaklamani DI (2004) Error estimation and optimization of the method of auxiliary sources (MAS) applied to TE scattering by a perfectly conducting circular cylinder. J Electromagn Waves Appl 18:1283–1294
11. Tsitsas NL, Alivizatos EG, Anastassiu HT, Kaklamani DI (2005) Optimization of the method of auxiliary sources (MAS) for scattering by an infinite cylinder under oblique incidence. Electromagnetics 25:39–54
12. Anastassiu HT (2005) Error estimation of the method of auxiliary sources (MAS) for scattering from an impedance circular cylinder. Prog Electromagn Res (PIER) 52:109–128
13. Anastassiu HT, Kaklamani DI (2004) Error estimation and optimization of the method of auxiliary sources (MAS) for scattering from a dielectric circular cylinder. Radio Science 39:RS5015, DOI: 1029/2004RS003028
14. Heretakis II, Papakanellos PJ, Capsalis CN (2002) Analysis of electromagnetic scattering by infinite conducting cylinders of arbitrary smooth cross section using a genetically optimised technique (GA/MAS). J Electromagn Waves Appl 16:1555–1572
15. Larsen NV, Breinbjerg O (2004) An analytical method of auxiliary sources solution for plane wave scattering by impedance cylinders-a reference solution for the numerical method of auxiliary sources. J Electromagn Waves Appl 18:745–761
16. Heretakis I, Papakanellos PJ, Capsalis CN (2005) A Stochastically optimized adaptive procedure for the location of MAS auxiliary monopoles: the case of electromagnetic scattering by dielectric cylinders. IEEE Trans Antennas Propagation 53:938–947
17. Balanis CA (1989) Advanced engineering electromagnetics. Wiley, New York
18. Tai CT (1994) Dyadic green functions in electromagnetic theory. IEEE Press, Piscataway
19. Warnick KF, Chew WC (2000) Accuracy of the method of moments for scattering by a cylinder. IEEE Trans Microwave Theory Tech 48:1652–1660
20. Davis PJ (1979) Circulant matrices. Wiley, New York